Energy-Resolved Information Scrambling in Energy-Space Lattices

S. Pegahan, I. Arakelyan, and J. E. Thomas

Phys. Rev. Lett. **126**, 070601 — Published 19 February 2021

DOI: 10.1103/PhysRevLett.126.070601

Energy-Resolved Information Scrambling in Energy-Space Lattices

S. Pegahan, I. Arakelyan and J. E. Thomas
[1] *Department of Physics, North Carolina State University, Raleigh, NC 27695, USA*
(Dated: December 10, 2020)

Weakly interacting Fermi gases simulate spin-lattices in energy-space, offering a rich platform for investigating information spreading and spin coherence in a large many-body quantum system. We show that the collective spin vector can be determined as a function of energy from the measured spin density, enabling general energy-space resolved protocols. We measure an out-of-time-order correlation function in this system and observe the energy dependence of the many-body coherence.

Trapped, weakly interacting Fermi gases provide a new paradigm for the study of many-body physics in a large quantum system containing $N \simeq 10^5$ atoms with a tunable, reversible Hamiltonian [1, 2]. In this system, coherent superpositions of two hyperfine states behave as pseudo-spins and the s-wave scattering length is magnetically tuned to nearly vanish [1, 3, 4]. The corresponding collision rate is negligible, so that single atom energies are conserved [1, 5–7] over the experimental time scale. The conserved single particle energy states label the "sites" of an effective energy-space lattice, simulating a variety of spin-lattice models [8]. Interactions are effectively long range in energy-space [4, 8, 9], important for new studies of information scrambling in a far from equilibrium, nearly zero temperature regime [10] and for applications to fast scrambling [11] and "out-of-equilibrium" dynamics in spin-lattice systems [12]. However, measurements in weakly interacting Fermi gases [1–7] have been limited to the spatial profiles of the collective spin density or the total number of atoms in each spin state, precluding observation of many-body correlations in chosen sectors of the energy-space lattice.

Of particular interest is the measurement of out-of-time-order correlation (OTOC) functions in weakly interacting Fermi gases. Certain OTOC functions [13–16] can serve as entanglement witnesses and to quantify coherence and information scrambling in quantum many-body systems [10, 17]. Originally, OTOC measurements were performed by reversing the time evolution of the many-body state in nuclear magnetic resonance experiments at high temperatures, where the initial state is described by a density operator and high order quantum coherence was observed [18]. New OTOC studies have been done in trapped ion systems containing relatively small numbers of atoms, where the individual sites are nearly equivalent, and the initial state is pure [10]. Related methods have been developed for systems containing up to 100 atoms [19], but the application of OTOC measurement to trapped ultracold gases has remained a challenge.

In this Letter, we report the demonstration of a general method for performing energy-resolved measurements of the collective spin vector in a harmonically-trapped weakly-interacting Fermi gas. We show that OTOC measurements can be implemented in this system and we extract many-body coherence in energy-resolved sectors, paving the way for new protocols, such as time-dependent energy-space correlation measurements.

In the experiments [20], we begin with a degenerate cloud of ^{6}Li containing a total of $N = 6.5 \times 10^4$ atoms in a single spin state. The cloud is confined in a harmonic, cigar-shaped optical trap, with oscillation frequencies $\omega_x/2\pi = 23$ Hz along the cigar x-axis and $\omega_r/2\pi = 625$ Hz in the transverse (y, z) directions. The corresponding Fermi temperature $T_F = 0.73\,\mu$K and $T/T_F = 0.32$.

We employ the two lowest hyperfine-Zeeman states, which are denoted by $|1\rangle \equiv |\uparrow_z\rangle$ and $|2\rangle \equiv |\downarrow_z\rangle$. The cloud is initially prepared in state $|\downarrow_z\rangle$ in a bias magnetic field of 528.53 G, where the s-wave scattering length $a_{12} \equiv a = 4.24\,a_0$ [4]. In this case, the largest possible collision rate γ_c in the Fermi gas arises for an incoherent mixture with $N/2$ atoms in each of two spin states. We find $\gamma_c < 1.7 \times 10^{-3}\,\mathrm{s}^{-1}$ [21], which is negligible for the experimental time scale < 1 s. Hence, the single particle energies are conserved and the energy distribution is time independent, as observed in the experiments [4, 20].

The Hamiltonian for the confined weakly interacting Fermi gas can be approximated as a one-dimensional (1D) spin "lattice" in energy space [4],

$$H(a) = a \sum_{i,j\neq i} g_{ij}\, \mathbf{s}_i \cdot \mathbf{s}_j - \sum_i \Omega_i\, s_{zi} \tag{1}$$

where we take $\hbar \equiv 1$. We associate a "site" i with the energy $E_i = (n_i + 1/2)\, h\nu_x$ of an atom in the i$^{\text{th}}$ harmonic oscillator state along the cigar axis x. For each E_i, we define a dimensionless collective spin vector $\mathbf{s}_i = \sum_{\alpha_i} \mathbf{s}_{\alpha_i}$, where the sum over α_i includes the occupied transverse (n_y, n_z) states for fixed n_i. As $k_B T_F/\hbar\omega_x \simeq 650$, the average number of atoms at each site is $N/650 \simeq 100$ [22].

The first term in Eq. 1 is a site-to-site interaction, proportional to the s-wave scattering length a and to the overlap of the harmonic oscillator probability densities for colliding atoms, $g_{ij} \propto \int dx\, |\phi_{E_i}(x)|^2\, |\phi_{E_j}(x)|^2 \propto 1/\sqrt{|E_i - E_j|}$, which is an effective long range interaction in the energy lattice [4]. For a zero temperature Fermi gas, the average interaction energy is $a\bar{g} = 3.8\,\Omega_{MF}$ [23], where the mean field frequency [4] for our experimental parameters is $\Omega_{MF}/2\pi \simeq 0.5$ Hz, i.e., $a\bar{g}/2\pi \simeq 1.9$ Hz.

The second term in Eq. 1 is an effective site-dependent Zeeman energy, arising from the quadratic spatial variation of the bias magnetic field along x, which produces a spin-dependent harmonic potential. As $\omega_r/\omega_x = 27$, the corresponding effect on the transverse (y, z) motion

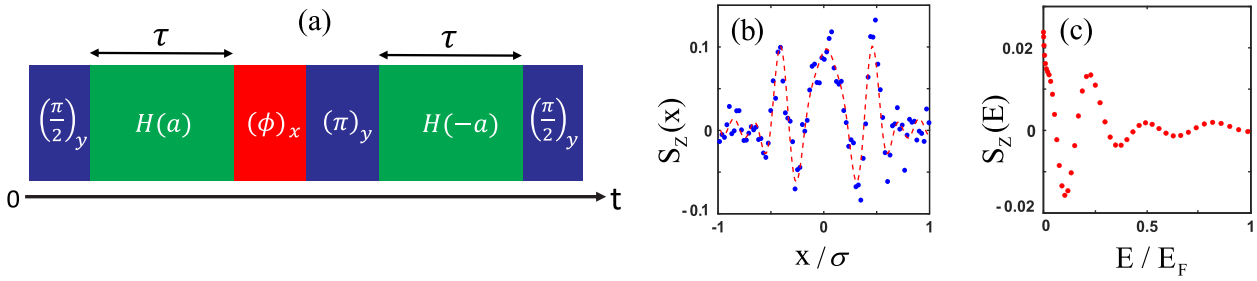

FIG. 1. Energy-resolved out-of-time-order correlation (OTOC) measurement. The system is initially prepared in a pure state, with the spins for atoms of energy $E_1, E_2, ...E_N$ polarized along the $-z$ axis; (a) OTOC sequence, after which the spatial profiles of the $\uparrow_z$ and $\downarrow_z$ states are measured for each cloud by resonant absorption imaging; (b) "single-shot" spin density profile $S_z(x)$ (blue dots). For this measurement, the scattering length in the Hamiltonian $H(a)$ is $a = 4.24\,a_0$, $\phi = \pi$, and $\sigma = 345\,\mu$m. (c) An inverse-Abel transform of the spatial profile (blue dots) extracts the single-shot energy-resolved spin density $S_z(E)$ (red dots). An Abel transform of $S_z(E)$ yields the red-dashed curve shown in (b), consistent with the data.

is negligible, so that all atoms at site i have the same Zeeman energy. In Eq. 1, $\Omega(E_i) \equiv \Omega_i = \Omega' E_i + \Delta'$, where $\Omega' = -\delta\omega_x/\hbar\omega_x$, with $\delta\omega_x/2\pi = 14.9$ mHz for our trap [4]. For atoms with the mean energy $\bar{E}_x \simeq k_B T_F/4$, $\Omega' \bar{E}_x/2\pi \simeq 2$ Hz. We define $\Delta' \equiv \Delta - \Omega' \bar{E}_x$, where Δ is the global detuning and $\Delta = 0$ corresponds to $\Omega_i = 0$ for the mean energy, $E_i = \bar{E}_x$.

A key feature of our experiments is the extraction of energy-resolved spin densities $n_{\uparrow_z,\downarrow_z}(E)$ by inverse Abel-transformation of the corresponding 1D spatial profiles $n_{\uparrow_z,\downarrow_z}(x)$, which are obtained from absorption images of a single cloud. The transform method requires a continuum approximation, which is justified for the x-direction, where $k_B T_F/\hbar\omega_x = 650$. Further, we require negligible energy space coherence, i.e., the atomic spins remain effectively localized in their individual energy sites. This assumption is justified by the very small transition matrix elements $< 10^{-4}\,\hbar\omega_x$ [24] between three dimensional harmonic oscillator states, which arise from short range interactions between two atoms [20].

In this regime, the spatial profile for each spin state $n_\sigma(x)$, $\sigma \equiv \uparrow_z, \downarrow_z$, is an Abel transform of the corresponding energy profile $n_\sigma(E)$ [20],

$$n_\sigma(x) = \int dE\, |\phi_E(x)|^2\, n_\sigma(E) = \frac{\omega_x}{\pi} \int_0^\infty dp_x\, n_\sigma\left(\frac{p_x^2}{2m} + \frac{m\omega_x^2}{2}x^2\right). \quad (2)$$

In Eq. 2, the last form is obtained by using a WKB approximation for the harmonic oscillator states $\phi_E(x)$ [20]. An inverse Abel-transform [20, 25] of $n_\sigma(x)$ then determines $n_\sigma(E)$ with a resolution $\Delta E \simeq 0.04\,E_F$ [20].

For the protocol of Fig. 1(a), discussed in detail below, Fig. 1(b) shows the measured *single-shot* spin density, $S_z(x,\phi) = [n_{\uparrow_z}(x,\phi) - n_{\downarrow_z}(x,\phi)]/2$, in units of the central total spin density $n(0)$. Fig. 1(c) shows the corresponding single-shot $S_z(E,\phi)$, obtained by inverse-Abel transformation of $S_z(x,\phi)$. We see that $S_z(E,\phi)$ appears smooth compared to the single-shot spin density $S_z(x,\phi)$, which requires averaging over several shots to obtain a smooth profile. To check that the inverse-Abel transform has adequate energy resolution, we Abel transform the extracted $S_z(E,\phi)$, yielding the red-dotted curve of Fig. 1(b), which is consistent with the measured density profile [20].

Our experimental OTOC protocol, Fig. 1(a), applies a rotation ϕ to the total interacting spin system in between forward and time-reversed evolutions. Then, a measurement of s_{zi} is performed to diagnose the effects of the rotation on the spins at "site i" in energy space. We start by preparing a fully z-polarized state $|\downarrow_{z1}\downarrow_{z2} ... \downarrow_{zN}\rangle \equiv |\psi_{z0}\rangle$ in a bias magnetic field $B_1 = 528.53$ G, where the scattering length $a_1 \equiv a = 4.24\,a_0$. Then we apply a 0.5 ms radio-frequency $(\pi/2)_y$ pulse (defined to be about the y-axis), which is resonant with the $|\downarrow_z\rangle \to |\uparrow_z\rangle$ transition at the bias field B_1, to produce an initial x-polarized N-atom state $|\psi_0\rangle = e^{-i\frac{\pi}{2}S_y}|\psi_{z0}\rangle = |\uparrow_{x1}\uparrow_{x2} ... \uparrow_{xN}\rangle$. The system evolves for a time $\tau = 200$ ms at the initial bias magnetic field $B_1 = 528.53$ G. Then, a resonant radio-frequency pulse $(\phi)_x$, shifted in phase from the first pulse by $\pi/2$, rotates the N-atom state about the x-axis [26] by a chosen angle ϕ. Immediately following this rotation, we reverse the sign of the Hamiltonian by applying a $(\pi)_y$ pulse and tuning the bias magnetic field to a value $B_2 = 525.83$ G, where the scattering length $a_2 = -a$, i.e., $e^{i\pi S_y} H(-a)\, e^{-i\pi S_y} = -H(a)$, from Eq. 1. After the system evolves for an additional time τ, the bias field is ramped back to B_1, and a final $(\pi/2)_y$ pulse is applied [20]. The final state of the N-atom system after the pulse sequence of Fig. 1(a) can be written as

$$|\psi_f\rangle = e^{-i\frac{3\pi}{2}S_y} W_\phi(\tau)|\psi_0\rangle, \quad (3)$$

where the W-operator is defined by

$$W_\phi(\tau) = e^{iH(a)\tau} e^{-i\phi\, S_x} e^{-iH(a)\tau}, \quad (4)$$

with $S_x = \sum_{i,\alpha_i} s_{x\alpha_i}$ the x-component of the *total* spin vector for the N-atom sample and $|\psi_0\rangle$ the fully x-polarized state. After the pulse sequence, the spin densities $n_{\uparrow_z}(x)$ and $n_{\downarrow_z}(x)$ are measured for a single cloud

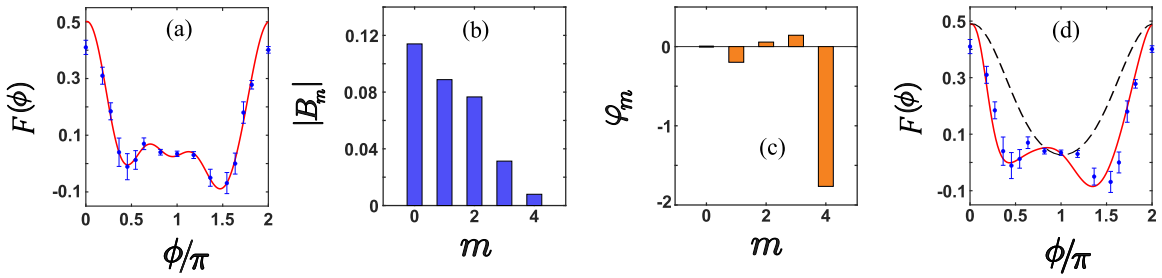

FIG. 2. Total collective spin projection S_z versus rotation angle ϕ without energy restriction. (a) $F(\phi) = \frac{1}{2}(N_{\uparrow_z} - N_{\downarrow_z})/(N_{\uparrow_z} + N_{\downarrow_z})$ (blue dots) for a measured scattering length $a_{\rm meas} = 4.24\,a_0$. The red solid curve is the fit of Eq. 8, which determines the magnitudes of the coherence coefficients $|B_m|$ (b) and corresponding phases φ_m (c); (d) Fit of the mean field model of Ref. [4] to the data (blue dots) for a global detuning $\Delta = 0$ with $a = a_{\rm meas}$ (black-dashed) and with $a = 2.63\,a_{\rm meas}$ (red-solid).

using two resonant absorption images, separated in time by $10\,\mu$s. We define one repetition of this experimental sequence as a "single-shot," in Fig. 1(b) and (c). Inverse-Abel transformation of $[n_{\uparrow z}(x) - n_{\downarrow z}(x)]/2$ then measures $S_z(E_i, \phi) \equiv s_{zi}$, for a single shot, Fig. 1(c).

Now we connect the measured s_{zi} to information scrambling [10, 13, 19]. Consider a *single spin* labelled by α_i, with spin components $s_{x\alpha_i}, s_{y\alpha_i}, s_{z\alpha_i}$, interacting with the many-body system. It is straightforward to show [20],

$$C_{\alpha_i} \equiv \langle\psi_0|[W_\phi(\tau), s_{x\alpha_i}]|^2|\psi_0\rangle = \frac{1}{2} - \langle\psi_f|s_{z\alpha_i}|\psi_f\rangle. \quad (5)$$

As the many-body operator W_ϕ and the single spin operator $s_{x\alpha_i}$ initially commute, i.e., $[W_\phi(0), s_{x\alpha_i}] = 0$, a measurement of $\langle\psi_f|s_{z\alpha_i}|\psi_f\rangle$ determines how two initially commuting operators fail to commute at a later time, providing a measure of scrambling.

In the experiments, we measure the *collective* spin operators $s_{zi} = \sum_{\alpha_i} s_{z\alpha_i}$, where $\alpha_i \equiv (n_i, n_y, n_z)$ for fixed n_i. The corresponding mean square commutator, averaged over the N_s spins with x-energy E_i, is [20]

$$\frac{1}{N_s}\sum_{\alpha_i} C_{\alpha_i}(\phi, \tau) = \frac{1}{2} - \frac{1}{N_s}\sum_{\alpha_i}\langle\psi_f|s_{z\alpha_i}|\psi_f\rangle. \quad (6)$$

Further averaging Eq. 6 over atoms with energies within ΔE of $E_i \equiv E$, we replace the sum on the righthand side by $S_z(E)\,\Delta E/[n(E)\,\Delta E]$, yielding the measured quantity

$$\mathcal{F}(E, \phi) \equiv \frac{1}{2}\,\frac{n_{\uparrow_z}(E, \phi) - n_{\downarrow_z}(E, \phi)}{n_{\uparrow_z}(E, \phi) + n_{\downarrow_z}(E, \phi)}. \quad (7)$$

Here, $n(E) = n_{\uparrow_z}(E, \phi) + n_{\downarrow_z}(E, \phi)$ is independent of ϕ and $\mathcal{F}(E, 0) = 1/2$.

We can extract information about the many-body coherence from Eq. 6, by writing the sum on the right-hand side as $\sum_m e^{im\phi} B_m$ [20]. Non-vanishing coefficients B_m correspond to coherence between states for which the x-component S_x of the total angular momentum differs by m [17, 20]. Since the sum is real, $B_{-m} = B_m^*$, we can expand Eq. 7 for the measured, energy-selected average in the form

$$\mathcal{F}(E, \phi) = B_0 + \sum_{m\geq 1} 2\,|B_m|\cos(m\phi + \varphi_m). \quad (8)$$

In fitting the data with Eq. 8, we restrict the range of m to 4. We find that the fits are not improved by further increase of m, consistent with the limited number of ϕ values measured in the experiments.

We measure spin density profiles $n_{\uparrow_z,\downarrow_z}(x, \phi)$ for a scattering length $a = 4.24\,a_0$. The data are averaged over 6 repetitions for each ϕ, with the ϕ values chosen in random order. We begin by finding the *total* number of atoms in each spin state $N_{\uparrow_z,\downarrow_z}(\phi) = \int dx\, n_{\uparrow_z,\downarrow_z}(x, \phi)$ for the protocol of Fig. 1(a), to find the total collective spin projection S_z versus rotation angle ϕ, *without* energy restriction. Fig. 2(a) shows the normalized S_z data $F(\phi) = \frac{1}{2}(N_{\uparrow_z} - N_{\downarrow_z})/(N_{\uparrow_z} + N_{\downarrow_z})$ (blue dots) and the fit of Eq. 8 (red curve), which determines the magnitude (b) and phase (c) of the average coherence coefficients B_m. We note that $F(0) \simeq F(2\pi) < 1/2$, the maximum for ideal conditions. This discrepancy arises from small variations in the phase shift of the final $\pi/2$ pulse, which is applied at a finite detuning as the magnetic field is ramped from B_2 back to its original value B_1 [20].

To check that the measurements are reasonable, we compare the ϕ-dependent data of Fig. 2 to a fit of our 1D mean field model, which employs a calculated average transverse density $\bar{n}_\perp$ to fit single-pulse spin-wave data with no free parameters [4]. The model, evaluated with a global detuning $\Delta = 0$, is shown in Fig. 2(d). To fit the observed ϕ dependence (red solid curve), the model requires a scattering length $a_{eff} \equiv 2.63\,a_{\rm meas}$, i.e., 2.63 times larger than the measured value $a_{\rm meas} = 4.24\,a_0$, which yields the black-dashed curve. The increased a_{eff} may occur because the measured coherence orders with $|m| > 1$ arise from interactions, favoring the largest couplings in a manner that is not predicted by our model.

Fig. 3 shows the energy-resolved measurements $\mathcal{F}(E, \phi)$, obtained by inverse-Abel transformation of the same data. The top row shows significant variation in symmetry and structure as the energy is varied from

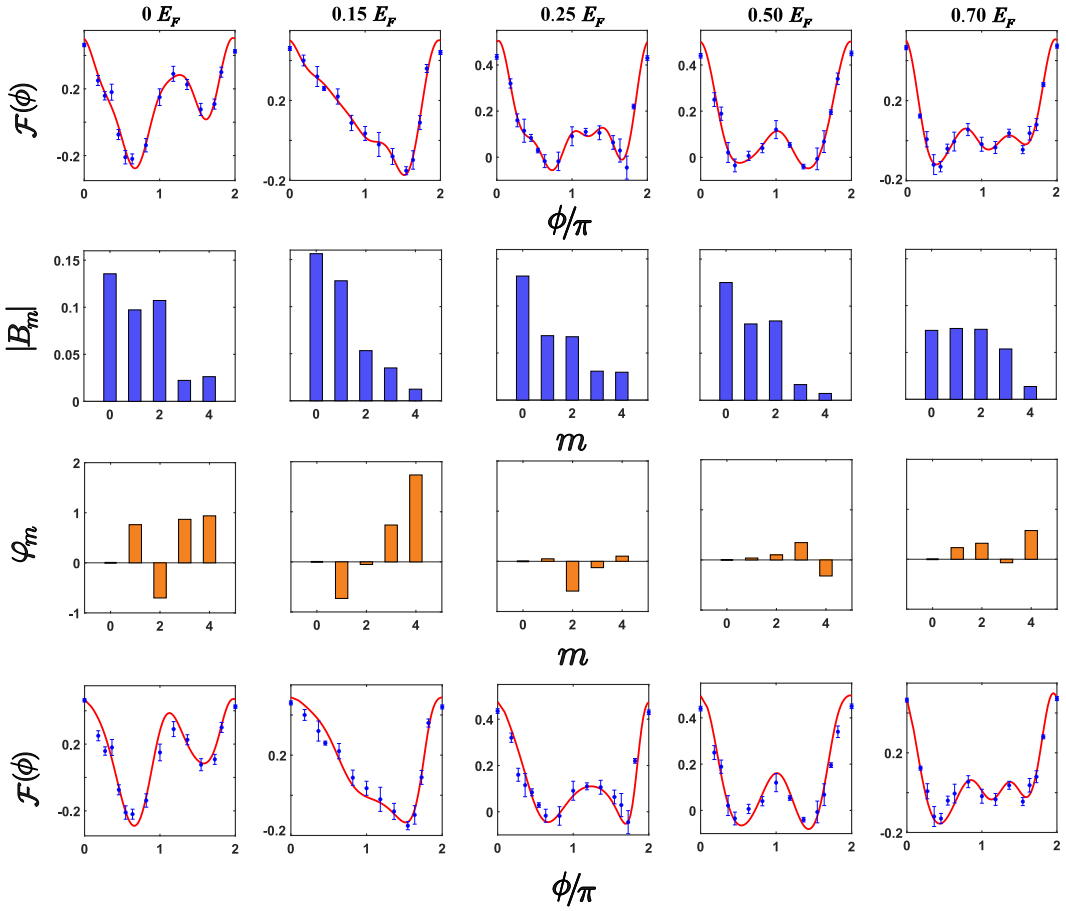

FIG. 3. Energy-resolved collective spin projection $S_z(E)$ versus rotation angle ϕ for spins of selected energies (left to right) $E/E_F = 0, 0.15, 0.25, 0.5, 0.7$. Here, $\mathcal{F}(\phi) = \frac{1}{2}[n_\uparrow(E) - n_\downarrow(E)]/[n_\uparrow(E) + n_\downarrow(E)]$. The top row shows the data (blue dots) for a measured scattering length $a = 4.24\,a_0$. The red solid curve is the fit of Eq. 8, which determines the magnitudes of the coherence coefficients $|B_m|$ (second row) and corresponding phases φ_m (third row); The bottom row shows the fits (red solid curves) of the mean field model of Ref. [4] to the data (blue dots), using a scattering length 2.63 times the measured value and global detunings, ordered in energy, of Δ(Hz) = 0, 0.8, 0.65, −0.8, and 0.15.

$E = 0$ to $E = 0.7\,E_F$. The red solid curves in the first row show the fit of Eq. 8, which yields the magnitudes of the coherence coefficients $|B_m|$ and the corresponding phases φ_m. In the last row, we compare the data to fits of the mean field model [4]. Again, the model captures the complex ϕ-dependent shapes of the data with $a_{eff} = 2.63\,a_{\rm meas}$, but a different detuning Δ is needed for each energy. This may be a consequence of averaging data over several detunings Δ, where each Δ rotates the direction of the ϕ-rotation axis by $\Delta\tau$ [26].

In summary, we have demonstrated a general method for measuring energy-resolved collective spin vectors in an energy-space lattice with effective long-range interactions. We have shown that an OTOC protocol can be implemented in this system and that many-body coherence can be measured in selected energy-space subsystems. Future measurement of time-dependent correlations between extensive subsets, $C_{ij}(t) \equiv \langle\psi_0|s_{xi}(t)s_{xj}(t)|\psi_0\rangle - \langle\psi_0|s_{xi}(t)|\psi_0\rangle\langle\psi_0|s_{xj}(t)|\psi_0\rangle$, enables a wide variety of protocols, extending correlation measurements in small numbers of trapped ions [27] to large quantum systems. For an initial x-polarized product state, $|\psi_0\rangle$, $C_{ij}(t) = 0$ for noninteracting systems and for our mean-field model, so that $C_{ij}(t) \neq 0$ signifies beyond mean-field physics. As $C_{ij}(0) = 0$, a scrambling time [28, 29] is determined by observing the evolution from the product state to a correlated state.

Primary support for this research is provided by the Air Force Office of Scientific Research (FA9550-16-1-0378) and the National Science Foundation (PHY-2006234). Additional support for the JETlab atom cooling group has been provided by the Physics Division of the Army Research Office (W911NF-14-1-0628) and by the Division of Materials Science and Engineering, the Office of Basic Energy Sciences, Office of Science, U.S. Department of Energy (DE-SC0008646).

*Corresponding author: jethoma7@ncsu.edu

[1] X. Du, Y. Zhang, J. Petricka, and J. E. Thomas, Controlling spin current in a trapped Fermi gas, Phys. Rev. Lett. **103**, 010401 (2009).

[2] S. Smale, P. He, B. A. Olsen, K. G. Jackson, H. Sharum, S. Trotzky, J. Marino, A. M. Rey, and J. H. Thywissen, Observation of a transition between dynamical phases in a quantum degenerate Fermi gas, Science Advances **5** (2019), elocation-id: eaax1568.

[3] X. Du, L. Luo, B. Clancy, and J. E. Thomas, Observation of anomalous spin segregation in a trapped Fermi gas, Phys. Rev. Lett. **101**, 150401 (2008).

[4] S. Pegahan, J. Kangara, I. Arakelyan, and J. E. Thomas, Spin-energy correlation in degenerate weakly interacting Fermi gases, Phys. Rev. A **99**, 063620 (2019).

[5] F. Piéchon, J. N. Fuchs, and F. Laloë, Cumulative identical spin rotation effects in collisionless trapped atomic gases, Phys. Rev. Lett. **102**, 215301 (2009).

[6] S. S. Natu and E. J. Mueller, Anomalous spin segregation in a weakly interacting two-component Fermi gas, Phys. Rev. A **79**, 051601 (2009).

[7] C. Deutsch, F. Ramirez-Martinez, C. Lacroûte, F. Reinhard, T. Schneider, J. N. Fuchs, F. Piéchon, F. Laloë, J. Reichel, and P. Rosenbusch, Spin self-rephasing and very long coherence times in a trapped atomic ensemble, Phys. Rev. Lett. **105**, 020401 (2010).

[8] A. P. Koller, M. L. Wall, J. Mundinger, and A. M. Rey, Dynamics of interacting fermions in spin-dependent potentials, Phys. Rev. Lett. **117**, 195302 (2016).

[9] U. Ebling, A. Eckardt, and M. Lewenstein, Spin segregation via dynamically induced long-range interactions in a system of ultracold fermions, Phys. Rev. A **84**, 063607 (2011).

[10] M. Gärttner, J. G. Bohnet, A. Safavi-Naini, M. L. Wall, J. J. Bollinger, and A. M. Rey, Measuring out-of-time-order correlations and multiple quantum spectra in a trapped-ion quantum magnet, Nature Physics **13**, 781 (2017).

[11] G. Bentsen, T. Hashizume, A. S. Buyskikh, E. J. Davis, A. J. Daley, S. S. Gubser, and M. Schleier-Smith, Treelike interactions and fast scrambling with cold atoms, Phys. Rev. Lett. **123**, 130601 (2019).

[12] J. Eisert, M. Friesdorf, and C. Gogolin, Quantum many-body systems out of equilibrium, Nature Phys. **11**, 124 (2015).

[13] M. Schleier-Smith, Probing information scrambling, Nature Physics **13**, 724 (2017).

[14] B. Swingle and N. Y. Yao, Seeing scrambled spins, Physics **10**, 82 (2017).

[15] J. Li, R. Fan, HengyanWang, B. Ye, B. Zeng, H. Zhai, X. Peng, and J. Du, Measuring out-of-time-order correlators on a nuclear magnetic resonance quantum simulator, Phys. Rev. X **7**, 031011 (2017).

[16] J. Marino and A. M. Rey, Cavity-qed simulator of slow and fast scrambling, Phys. Rev. A **99**, 051803 (2019).

[17] M. Gärttner, P. Hauke, and A. M. Rey, Relating out-of-time-order correlations to entanglement via multiple-quantum coherences, Phys. Rev. Lett. **120**, 040402 (2018).

[18] J. Baum, M. Munowitz, A. N. Garroway, and A. Pines, Multiple-quantum dynamics in solid state NMR, The Journal of Chemical Physics **83**, 2015 (1985).

[19] R. J. Lewis-Swan, A. Safavi-Naini, J. J. Bollinger, and A. M. Rey, Unifying scrambling, thermalization and entanglement through measurement of fidelity out-of-time-order correlators in the Dicke model, Nature Communications **10**, 5007 (2019).

[20] See Supplemental Material for a description of the experimental details and of the inverse Abel-transform method.

[21] M. E. Gehm, S. L. Hemmer, K. M. O'Hara, and J. E. Thomas, Unitarity-limited elastic collision rate in a harmonically trapped Fermi gas, Phys. Rev. A **68**, 011603 (2003).

[22] The number of atoms Δn_i at site i, i.e., in x-mode E_i, summed over y, z transverse modes, is $\Delta n_i \simeq \frac{3\,\Delta E_i\,N}{E_F}(1-E_i/E_F)^2$. With $\Delta E_i = \hbar\omega_x$, $N = 6.5\times10^4$, and $E_i = E_F/2$, we find $\Delta n_i \simeq 74$.

[23] Here, we employ a continuum approximation with $\bar{g} \equiv \int dn P(n) \int dn' P(n') g(n,n')$, in the notation of Ref. [4].

[24] Nonzero matrix elements arise for transitions between states of relative motion with *even* x-quantum number $2n$ and azimuthal quantum number $l = 0$ [20]. For our trap, $\sqrt{\hbar/m\omega_x} \simeq 8.5\,\mu$m and $\nu_r/\nu_x = 27$. With $a = 4.24\,a_0$, $\langle 2n', m_r'|H'|2n, m_r\rangle/h\nu_x \simeq 3.2\times10^{-4}/(n'\,n)^{1/4}$, independent of the radial quantum numbers m_r, m_r'.

[25] G. Pretzier, A new method for numerical Abel-inversion, Zeitschrift fr Naturforschung A **46**, 639 (1991).

[26] Note that a nonzero detuning Δ changes the effective axis of rotation to $\hat{e}_{x'} = \cos(\Delta\tau)\,\hat{e}_x + \sin(\Delta\tau)\,\hat{e}_y$ without changing the general ϕ-dependent structure of the OTOC [20].

[27] P. Richerme, Z.-X. Gong, A. Lee, C. Senko, J. Smith, M. Foss-Feig, S. Michalakis, A. V. Gorshkov, and C. Monroe, Non-local propagation of correlations in quantum systems with long-range interactions, Nature **511**, 198 (2014).

[28] A. Y. Guo, M. C. Tran, A. M. Childs, A. V. Gorshkov, and Z.-X. Gong, Signaling and scrambling with strongly long-range interactions, Phys. Rev. A **102**, 010401 (2020).

[29] J. Maldacena, S. H. Shenker, and D. Stanford, A bound on chaos, Journal of High Energy Physics **2016**, 106 (2016).